



**HAL**  
open science

## Multi-resonant absorption in ultra-thin silicon solar cells with metallic nanowires

I. Massiot, Clément Colin, Christophe Sauvan, Philippe Lalanne, Pere Roca I Cabarrocas, Jean-Luc Pelouard, Stéphane Collin

► **To cite this version:**

I. Massiot, Clément Colin, Christophe Sauvan, Philippe Lalanne, Pere Roca I Cabarrocas, et al.. Multi-resonant absorption in ultra-thin silicon solar cells with metallic nanowires. *Optics Express*, 2013, 21 (S3), pp.A372-A381. 10.1364/OE.21.00A372 . hal-00811652

**HAL Id: hal-00811652**

**<https://hal-iogs.archives-ouvertes.fr/hal-00811652>**

Submitted on 10 Apr 2013

**HAL** is a multi-disciplinary open access archive for the deposit and dissemination of scientific research documents, whether they are published or not. The documents may come from teaching and research institutions in France or abroad, or from public or private research centers.

L'archive ouverte pluridisciplinaire **HAL**, est destinée au dépôt et à la diffusion de documents scientifiques de niveau recherche, publiés ou non, émanant des établissements d'enseignement et de recherche français ou étrangers, des laboratoires publics ou privés.

# Multi-resonant absorption in ultra-thin silicon solar cells with metallic nanowires

Inès Massiot,<sup>1</sup> Clément Colin,<sup>1,2</sup> Christophe Sauvan,<sup>3</sup> Philippe Lalanne,<sup>3</sup> Pere Roca i Cabarrocas,<sup>4</sup> Jean-Luc Pelouard,<sup>1</sup> and Stéphane Collin<sup>1,\*</sup>

<sup>1</sup>Laboratoire de Photonique et de Nanostructures (LPN-CNRS), Route de Nozay, 91460 Marcoussis, France

<sup>2</sup>Institut de Recherche et Développement sur l'Energie Photovoltaïque (IRDEP), UMR 7174 CNRS/EDF/Chimie-ParisTech, 6 quai Watier, 78401 Chatou, France

<sup>3</sup>Laboratoire Photonique, Numérique et Nanosciences (LP2N), Université Bordeaux 1/CNRS/Institut d'Optique, 33405 Talence Cedex, France

<sup>4</sup>Laboratoire de Physique des Interfaces et Couches Minces (LPICM-CNRS), Ecole Polytechnique, 91128 Palaiseau Cedex, France

\*[stephane.collin@lpn.cnrs.fr](mailto:stephane.collin@lpn.cnrs.fr)

**Abstract:** We propose a design to confine light absorption in flat and ultra-thin amorphous silicon solar cells with a one-dimensional silver grating embedded in the front window of the cell. We show numerically that multi-resonant light trapping is achieved in both TE and TM polarizations. Each resonance is analyzed in detail and modeled by Fabry-Perot resonances or guided modes via grating coupling. This approach is generalized to a complete amorphous silicon solar cell, with the additional degrees of freedom provided by the buffer layers. These results could guide the design of resonant structures for optimized ultra-thin solar cells.

© 2013 Optical Society of America

**OCIS codes:** (040.5350) Photovoltaic; (050.6624) Subwavelength structures; (250.5403) Plasmonics; (350.4238) Nanophotonics and photonic crystals; (040.6040) Silicon.

---

## References and links

1. S. Benagli, D. Borrello, E. Vallat-Sauvain, J. Meier, U. Kroll, J. Hötzel, J. Bailat, J. Steinhauser, M. Marmelo, G. Monteduro, and L. Castens, "High-efficiency amorphous silicon devices on LPCVD-ZnO TCO prepared in industrial KAI-M R&D reactor," in *Proceedings of the 24th European Photovoltaic Solar Energy Conference* (Hamburg, 2009), pp. 2293–2298.
2. P. Campbell and M. A. Green, "The limiting efficiency of silicon solar cells under concentrated light," *IEEE Trans. Electron. Dev.* **33**(2), 234–239 (1986).
3. D. L. Staebler and C. R. Wronski, "Optically induced conductivity changes in discharge-produced hydrogenated amorphous silicon," *J. Appl. Phys.* **51**(6), 3262–3268 (1980).
4. B. Rech and H. Wagner, "Potential of amorphous silicon for solar cells," *Appl. Phys. A* **69**, 155–167 (1999).
5. J. Krc, F. Smole, and M. Topic, "Potential of light trapping in microcrystalline silicon solar cells with textured substrates," *Prog. Photovolt. Res. Appl.* **11**(7), 429–436 (2003).
6. C. Battaglia, K. Söderström, J. Escarré, F.-J. Haug, D. Dominé, P. Cuony, M. Boccard, G. Bugnon, C. Denizot, M. Despeisse, A. Feltrin, and C. Ballif, "Efficient light management scheme for thin film silicon solar cells via transparent random nanostructures fabricated by nanoimprinting," *Appl. Phys. Lett.* **96**, 213504 (2010).
7. K. Söderström, F. J. Haug, J. Escarré, O. Cubero, and C. Ballif, "Photocurrent increase in n-i-p thin film silicon solar cells by guided mode excitation via grating coupler," *Appl. Phys. Lett.* **96**, 213508 (2010).
8. A. Abass, K. Q. Lee, A. Alù, M. Burgelman, and B. Maes, "Dual-interface gratings for broadband absorption enhancement in thin-film solar cells," *Phys. Rev. B* **85**, 115449 (2012).
9. V. E. Ferry, M. A. Verschuuren, H. B. T. Li, E. Verhagen, R. J. Walters, R. E. I. Schropp, H. A. Atwater, and A. Polman, "Light trapping in ultrathin plasmonic solar cells," *Opt. Express* **18**, A237–A245 (2010).

10. V. E. Ferry, M. A. Verschuuren, C. van Lare, R. E. I. Schropp, H. A. Atwater, and A. Polman, "Optimized spatial correlations for broadband light trapping nanopatterns in high efficiency ultrathin film a-Si:H solar cells," *Nano Lett.* **11**(10), 4239–4245 (2011).
11. J. Zhu, C. M. Hsu, Z. Yu, S. Fan, and Y. Cui, "Nanodome solar cells with efficient light management and self-cleaning," *Nano Lett.* **10**, 1979–1984 (2010).
12. T. Söderström, F.J. Haug, V. Terrazoni-Daudrix, and C. Ballif, "Optimization of amorphous silicon thin film solar cells for flexible photovoltaics," *J. Appl. Phys.* **103**, 114509 (2008).
13. M. Python, O. Madani, D. Dominé, F. Meillaud, E. Vallat-Sauvain, and C. Ballif, "Influence of the substrate geometrical parameters on microcrystalline silicon growth for thin-film solar cells," *Sol. Energ. Mater. and Sol. Cells* **93**, 1714–1720 (2009).
14. K. R. Catchpole and A. Polman, "Design principles for particle plasmon enhanced solar cells," *Appl. Phys. Lett.* **93**, 191113 (2008).
15. F. J. Beck, A. Polman, and K. R. Catchpole, "Tunable light trapping for solar cells using localized surface plasmons," *J. Appl. Phys.* **105**, 114310 (2009).
16. O. El Daif, L. Tong, B. Figeys, K. Van Nieuwenhuysen, A. Dmitriev, P. Van Dorpe, and F. Dross, "Front side plasmonic effect on thin silicon epitaxial solar cells," *Sol. Energ. Mater. and Sol. Cells* **104**, 58–63 (2012).
17. M. van Lare, F. Lenzmann, M. A. Verschuuren, and A. Polman, "Mode coupling by plasmonic surface scatterers in thin-film silicon solar cells," *Appl. Phys. Lett.* **101**, 221110 (2012).
18. Y.-M. Chi, H.-L. Chen, Y.-S. Lai, H.-M. Chang, Y.-C. Liao, C.-C. Cheng, S.-H. Chen, S.-C. Tseng, and K.-T. Lin, "Optimizing surface plasmon resonance effects on finger electrodes to enhance the efficiency of silicon-based solar cells," *Energy Environ. Sci.* **6**, 935–942 (2013).
19. I. Massiot, C. Colin, N. Péré-Laperme, P. Roca i Cabarrocas, C. Sauvan, P. Lalanne, J.-L. Pelouard, and S. Collin, "Nanopatterned front contact for broadband absorption in ultra-thin amorphous silicon solar cells," *Appl. Phys. Lett.* **101**, 163901 (2012).
20. H. A. Atwater and A. Polman, "Plasmonics for improved photovoltaic devices," *Nat. Mater.* **9**(3), 205–213 (2010).
21. M. A. Green and S. Pillai, "Harnessing plasmonics for solar cells," *Nat. Photon.* **6**, 130–132 (2012).
22. M. G. Moharam, E. B. Grann, D. A. Pommert, and T. K. Gaylord, "Formulation for stable and efficient implementation of the rigorous coupled-wave analysis of binary gratings," *J. Opt. Soc. Am. A* **12**, 1068–1076 (1995).
23. P. Lalanne and G. M. Morris, "Highly improved convergence of the coupled-wave method for TM polarization," *J. Opt. Soc. Am. A* **13**, 779–789 (1996).
24. A free version of the software "Reticolo" is available at <http://www.lp2n.institutoptique.fr/Membres-Services/Responsables-d-equipe/LALANNE-Philippe>.
25. P. Lalanne and M. P. Jurek, "Computation of the near-field pattern with the coupled-wave method for TM polarization," *J. Mod. Opt.* **45**, 1357–1374 (1998).
26. E. D. Palik, *Handbook of Optical Constants of Solids* (Academic, 1985), pp. 350–357.
27. F.-J. Haug, T. Söderström, O. Cubero, V. Terrazoni-Daudrix, and C. Ballif, "Influence of the ZnO buffer on the guided mode structure in Si/ZnO/Ag multilayers," *J. Appl. Phys.* **106**, 044502 (2009).
28. A. Cattoni, P. Ghenuche, A. M. Haghiri-Gosnet, D. Decanini, J. Chen, J. L. Pelouard, and S. Collin, " $\lambda^3/1000$  plasmonic nanocavities for biosensing fabricated by soft UV nanoimprint lithography," *Nano Lett.* **11**, 3557–3563 (2011).

---

## 1. Introduction

Thin film solar cells are a promising solution to reduce the overall cost of photovoltaic cells and increase production rates. In particular, remarkable progress has been made in amorphous silicon (a-Si:H) solar cells technology leading to stable energy conversion efficiencies of 10% with 250 nm thick a-Si:H [1]. Reducing further the absorber layer thickness towards ultra-thin ( $\leq 100$  nm) a-Si:H solar cells should improve the collection of current in the cell [2] as well as the stability against light-induced degradation [3, 4]. However, advanced light trapping strategies are needed to overcome the poor light absorption in thin semiconductor layers. Conventionally, random texturing of the interfaces [5, 6] is used to enhance the optical path length but is incompatible with ultra-thin absorber layers. Numerous works have been done on light trapping through periodic nanopatterning of the back contact of the cell [7–11]. However, the growth of amorphous silicon on textured substrates leads to a reduction of the open-circuit voltage of the device because of the formation of cracks [12, 13]. Metallic nanostructures have also been integrated at the front surface of the cell to scatter light in crystalline [14–16] or amorphous [17] silicon solar cells, or to realize partially transparent electrodes [18].

To achieve efficient a-Si:H photovoltaic devices, our objective is to design a light trapping scheme that would allow flat and very thin ( $\leq 100$  nm) a-Si:H absorbers. In a previous work, we have proposed a design based on an array of 1D silver wires embedded in an anti-reflection coating layer deposited on an ultra-thin amorphous silicon cell with a silver back mirror [19]. We proposed to use the nanopatterned metallic front layer as an alternative to the conventional transparent conductive oxide (TCO) front contact in order to reduce the absorption losses at short wavelengths. A theoretical short-circuit current density of  $14.6 \text{ mA/cm}^2$  was numerically demonstrated at normal incidence for a 90 nm-thick a-Si:H layer, with low polarization and angle dependencies. In this design, broadband absorption stems from multi-resonant light trapping. The absorption spectrum can be tuned by varying the different parameters of the structure. The origin of each absorption peak still needs to be carefully understood.

Here, we provide an in-depth analysis of the resonances involved in the multi-resonant light-trapping mechanism. We first consider a simple three-layer model based on a TCO/a-Si:H/Ag stack with a 1D silver grating embedded in the top TCO layer. Numerical simulations were performed using an exact RCWA method [22–24]. For TM polarization (magnetic field parallel to the wires), a semi-analytical treatment is used for the calculation of the fields and the absorption [25]. The role of each key parameter of the structure (TCO layer thickness, a-Si:H thickness and grating period) in the absorption is analyzed. We apply this multi-resonant approach to the design of a complete solar cell with two buffer layers giving additional degrees of freedom to optimize further the absorption in the cell. This work can be generalized to other thin-film materials in order to conceive ultra-thin solar cells with resonant light trapping designs.

## 2. Design of 1D plasmonic nanostructures for ultra-thin a-Si:H solar cells

We consider a simplified three-layer structure, see Fig. 1(a). Light confinement is achieved with a 1D metallic grating (width  $w$ , pitch  $p$ , metal thickness  $h_m$ ) deposited on an amorphous silicon absorber layer (thickness  $h_s$ ) and a metallic mirror as a back contact. In amorphous silicon solar cells, the TCO layer is conventionally made of indium tin oxide (ITO) or aluminum doped zinc oxide (ZnO:Al). In the following, we considered ZnO:Al only. The top ZnO:Al layer (thickness  $h_1$ ) is used both as an anti-reflection coating layer and as a front contact. We define a structure based on an a-Si:H absorber layer with a thickness  $h_s = 90$  nm and a patterned silver layer ( $h_m = 20$  nm) embedded in a TCO layer ( $h_1 = 60$  nm). The corresponding metallic grating consists of silver wires with  $w = 80$  nm and  $p = 200$  nm. This structure will be used as a reference for the analysis developed in the following.

The refractive index of silver is taken from Ref. [26]. The refractive indices of a-Si:H ( $n_s$ ) and ZnO:Al ( $n_1$ ) have been measured by ellipsometry.

The calculated optical response of the reference structure at normal incidence is shown in Fig. 1(b). Broadband absorption is achieved for both TE and TM light polarizations. Remarkably, despite the strong anisotropy of the structure, high performance is achieved for both polarizations. This is due to the presence of six resonances (three for each polarization) that are judiciously combined by the design. The main absorption peaks identified in this structure are  $\lambda_{A_E} = 476$  nm,  $\lambda_{B_E} = 631$  nm,  $\lambda_{C_E} = 687$  nm for TE and  $\lambda_{A_M} = 430$ –550 nm,  $\lambda_{B_M} = 537$  nm,  $\lambda_{C_M} = 649$  nm for TM light polarizations. In the following section, we analyze the physical origin of the resonances.

For the sake of simplicity, only the total absorption spectrum is analyzed in section 3. Note that it enables to show resonances that would not contribute to the generation of current because they are below the energy bandgap. The absorption fraction in each layer of the stack is detailed in section 4 for a complete amorphous silicon solar cell. It shows that the same peak positions are obtained for the absorption in each part of the cell.

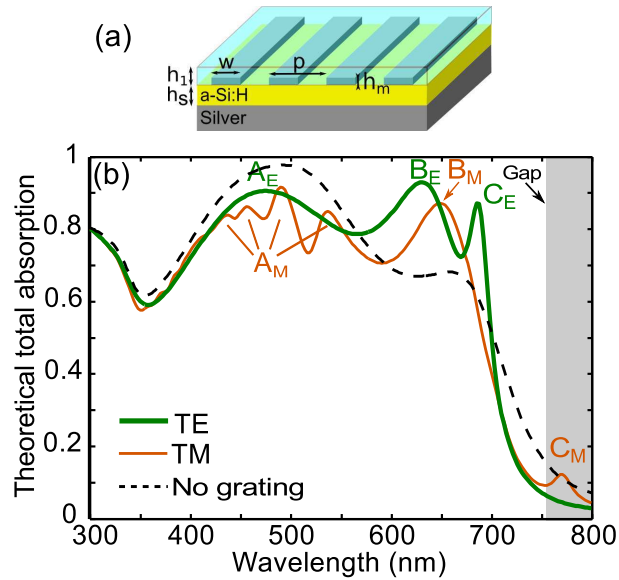


Fig. 1. (a) Schematic of the simplified structure made of a ZnO:Al/a-Si:H/Ag stack. A 1D silver grating (width  $w$ , pitch  $p$ , metal thickness  $h_m$ ) is deposited on the a-Si:H layer (thickness  $h_s$ ) and embedded in a ZnO:Al anti-reflection coating layer (thickness  $h_1$ ). (b) Spectra of the numerically computed total absorption of the reference structure under TM (orange) and TE (green) polarized light at normal incidence. The parameters of the metallic grating are  $p=200$  nm,  $w=80$  nm and  $h_m=20$  nm. The total absorption spectrum of a planar ZnO:Al (50 nm)/a-Si:H (90 nm)/Ag structure is shown with the black dashed curve for the sake of comparison.

### 3. Analysis of the multi-resonant absorption mechanism

In this section, we provide a physical analysis of the multi-resonant mechanism. To do so, we numerically study the evolution of the total absorption spectrum as a function of three important design parameters (ZnO:Al and a-Si:H thicknesses and the grating period) and we propose a simple analytical model to fit the numerical results.

#### 3.1. Absorption resonances in the top ZnO:Al layer: resonances $A_E$ & $A_M$

Let us consider the absorption peaks observed at short wavelengths (resonances  $A_E$  and  $A_M$ ). We first study the evolution of the absorption spectrum when the thickness  $h_1$  of the ZnO:Al layer varies from 20 to 170 nm. For  $h_1=20$  nm, the ZnO:Al exactly fills the grooves. Figure 2 displays the total absorption spectrum in the structure as a function of the ZnO:Al layer thickness  $h_1$ . At long wavelengths ( $\lambda > 600$  nm), absorption bands independent of  $h_1$  are attributed to resonances  $B_E$ ,  $C_E$ ,  $B_M$  and  $C_M$  as shown with orange dashed lines in Figs. 2(b) and 2(c). At shorter wavelengths ( $\lambda < 600$  nm), the TE and TM absorption diagrams exhibit two absorption bands (black dashed curves) that strongly depend on the ZnO:Al layer thickness.

We consider the top ZnO:Al layer as an asymmetric Fabry-Perot resonator with  $\phi_1$  and  $\phi_2$  the phase shifts induced by reflection at the ZnO:Al/Air and ZnO:Al/a-Si:H interfaces as depicted in Fig. 2(a). The influence of the metallic grating is neglected as a first approximation. In the Fabry-Perot model, the resonance condition in such a cavity can be written as

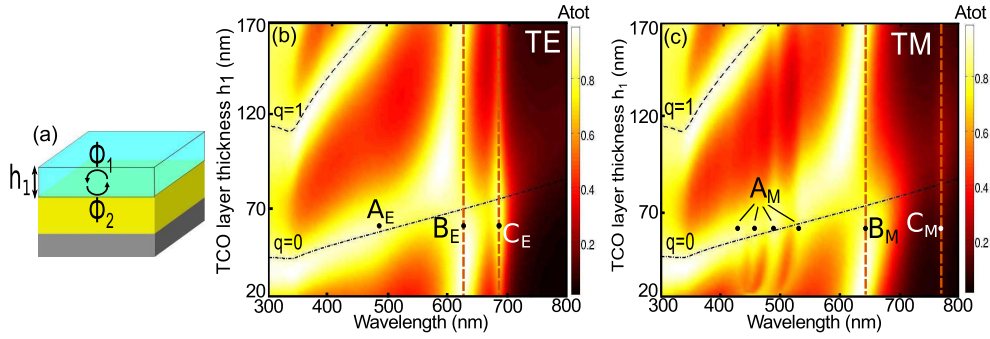


Fig. 2. Study of the short wavelengths resonances ( $A_E$ ) (TE) and ( $A_M$ ) (TM). (a) Sketch of the asymmetric Fabry-Perot resonator model used to fit the numerical calculations. The influence of the metallic grating is neglected.  $\phi_1$  and  $\phi_2$  are the phase shifts induced by reflection at the ZnO:Al/Air and ZnO:Al/a-Si:H interfaces. (b, c) Total light absorption spectrum in the simplified structure depicted in Fig. 1 as a function of the wavelength and the ZnO:Al layer thickness  $h_1$ . Excitation at normal incidence light in (b) TE and (c) TM polarizations. The position of the absorption bands with low dependence on  $h_1$  can be attributed to resonances  $B_E$ ,  $C_E$ ,  $B_M$  and  $C_M$  as shown with orange dashed lines. The resonance position  $h_1 = f(\lambda)$  given by the Fabry-Perot model (Eq.( 1)) is shown with black dashed curves for  $q = 0, 1$ .

$$h_1 = \frac{\lambda}{2n_1} \left( q - \frac{\varphi}{2\pi} \right) \quad (1)$$

with  $n_1$  the refractive index of the ZnO:Al layer and  $q$  an integer. The total phase shift  $\varphi$  is defined by  $\varphi = \phi_1 + \phi_2$ . From numerical calculations, we find that  $\phi_1$  and  $\phi_2$  vary slowly in the vicinity of the resonances. Thus, we use a constant value for  $\varphi$  in the Fabry-Perot model ( $\varphi \sim -1.89$  rad). The corresponding curves  $h_1 = f(\lambda)$  obtained from Eq. (1) with  $q = 0, 1$  are shown in Figs. 2(b) and 2(c) with black dashed curves. The latter remarkably well predict the absorption bands of the structure. The resonances  $A_E$  and  $A_M$  can thereby be attributed to the lowest order mode ( $q = 0$ ) of the Fabry-Perot resonances in the cavity Air/ZnO:Al/a-Si:H. Note that the Fabry-Perot resonance occurs in the ZnO:Al layer but leads to absorption in the active a-Si:H layer.

At short wavelengths (450-500 nm), the metallic grating has a minor effect on the optical response of the device in TM polarization, giving rise to a splitting of the resonance  $A_M$ . As shown in Fig. 2, the error in the spectral position of the peaks with respect to the Fabry-Perot model increases with the wavelength.

### 3.2. Absorption resonances in the a-Si:H layer: resonances $B_E$ & $B_M$

The nature of resonances  $B_E$  and  $B_M$  is now investigated. Figure 3 displays the evolution of the predicted total absorption under (b) TE and (c) TM polarizations as a function of the absorber layer thickness  $h_s$ . We first note that  $h_s$  has only a minor influence on the absorption bands discussed in section 3.1, in agreement with the Fabry-Perot interpretation of Air/ZnO:Al/a-Si:H resonances. On the contrary, according to Figs. 3(b) and 3(c), the absorption peaks corresponding to  $B_E$  and  $B_M$  have a spectral position and an intensity that both strongly depend on  $h_s$ . We thereby consider an asymmetric Fabry-Perot resonator (see Fig. 3(a)) and we can adapt the resonance condition of Eq. (1) with  $h_1 = h_s$  and  $n_1 = n_s$ . As in the previous subsection, the influence of the metallic grating is neglected and we use a constant value for  $\varphi$  ( $\varphi \sim -1.82$  rad).

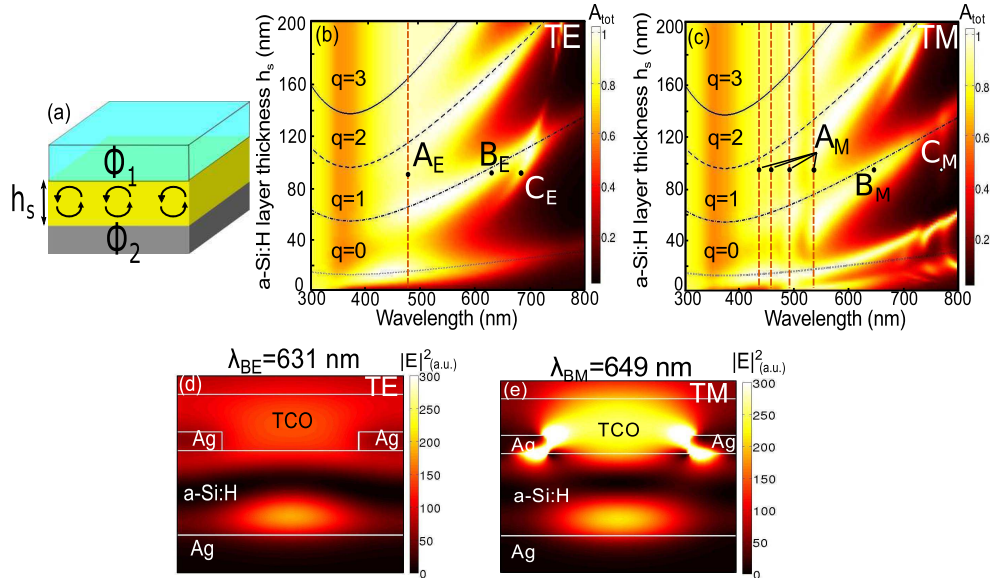


Fig. 3. Study of the resonances ( $B_E$ ) (TE) and ( $B_M$ ) (TM). (a) Sketch of the asymmetric Fabry-Perot resonator model used to fit the numerical calculations. The influence of the metallic grating is neglected.  $\phi_1$  and  $\phi_2$  are the phase shifts induced by reflection at the a-Si:H/ZnO:Al and a-Si:H/Ag interfaces. (b, c) Total light absorption spectrum in the simplified structure depicted in Fig. 1 as a function of the wavelength and the absorber layer thickness  $h_s$ . Excitation at normal incidence light in (b) TE and (c) TM polarizations. The resonance position  $h_s = f(\lambda)$  given by the Fabry-Perot model (Eq. (1)) with  $h_1 = h_s$  and  $n_1 = n_s$ , is shown in black dashed lines for  $q = 0, 1, 2, 3$ . (d, e) Electric field intensity maps for a 1D silver grating with  $w = 80$  nm,  $p = 200$  nm,  $h_m = 20$  nm for an excitation at (d)  $\lambda_{B_E} = 631$  nm under TE polarized light and (e)  $\lambda_{B_M} = 649$  nm under TM polarized light.

The corresponding curves  $h_s = f(\lambda)$  are plotted in Figs. 3(b) and 3(c) with black dashed lines for different values of the integer  $q$ . For both  $B_E$  and  $B_M$  resonances, the Fabry-Perot model is in qualitative agreement with the RCWA calculations. Both absorption peaks can thereby be attributed to Fabry-Perot resonances within the a-Si:H layer (mode with  $q = 0$ ).

Figures 3(d) and 3(e) display the spatial distribution of the electric field intensity between the silver strips when the structure is excited at  $\lambda = 631$  nm (TE, resonance  $B_E$ ) and  $\lambda = 649$  nm (TM, resonance  $B_M$ ). In TE polarization, the field maximum is located within the a-Si:H layer with a low field intensity in the metal. In the case of the resonance  $B_E$ , the effect of the metallic grating is thereby negligible. In TM polarization, there is a field exaltation on the edges of the silver. Consistently, there is a much larger difference between  $\lambda_{B_M}$  and the wavelength predicted by the Fabry-Perot model.

### 3.3. Absorption resonances induced by guided modes: resonances $C_E$ & $C_M$

The last resonance contributing to the absorption in the a-Si:H layer in TE polarization, called  $C_E$ , involves a different mechanism. We have investigated the influence of the angle of incidence  $\theta$  (plane of incidence perpendicular to the wires) and the grating period  $p$  on the absorption spectrum of the structure. The results are shown in Figs. 4(a) and 4(b). The absorption peak corresponding to the resonance  $C_E$  is the only one exhibiting a dispersive character as vary  $\theta$  and  $p$ . Figure 4(c) displays the spatial distribution of the electric field intensity for an

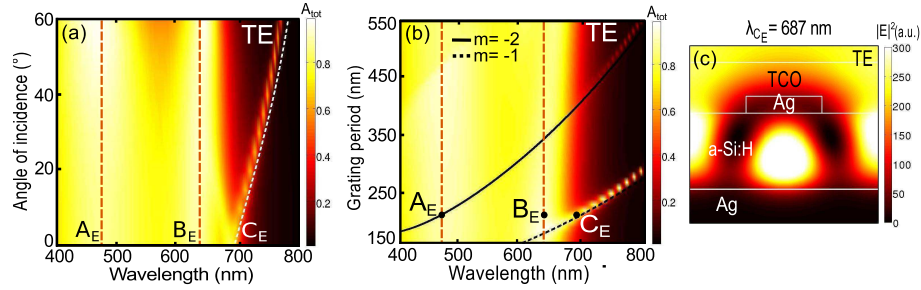


Fig. 4. Study of the long wavelength ( $C_E$ ) resonance for TE polarization. (a) Total light absorption spectrum as a function of the wavelength and the angle of incidence (plane of incidence perpendicular to the wires). (b) Total light absorption spectrum as a function of the wavelength and the grating period at normal incidence. The absorption bands attributed to resonances  $A_E$  and  $B_E$  are shown in orange dashed lines in Figs. 4 (a) and (b). (c) Electric field intensity map for an excitation at  $\lambda_{C_E} = 687$  nm for a TE polarization at normal incidence.

excitation at wavelength  $\lambda_{C_E}$  in TE polarization. The grating efficiently traps light because of the excitation of a waveguide mode supported by the a-Si:H layer as shown in previous studies on a-Si:H solar cells with periodic patterns [7, 9]. Indeed, the grating supplies an extra momentum so that the coupling of the incident light with a diffracted mode of order  $m$  could satisfy the conservation of the in-plane momentum and excite an eigenmode of the TCO/a-Si:H/Ag waveguide:

$$\frac{2\pi}{\lambda_{C_E}} \text{Re}(n_{eff}) = \left| \frac{2\pi}{\lambda_{C_E}} \sin \theta + m \frac{2\pi}{p} \right| \quad (2)$$

with  $m$  a relative integer and  $n_{eff}$  the effective index of the waveguide mode. Equation (2) is valid provided that one neglects the effective index change induced by the silver grating.

We consider the mode resulting from the coupling to the diffracted order  $m = -1$  and guided in the ZnO:Al/a-Si:H/Ag waveguide under TE polarization. Using Eq. (2), we have plotted the  $\theta = f(\lambda_{C_E})$  curve for the structure with  $p = 200$  nm in Fig. 4(a) (white dashed line). It agrees well with the shift of  $\lambda_{C_E}$  predicted by the RCWA calculations as  $\theta$  increases. We have also plotted the curve  $p = f(\lambda_{C_E})$  given by Eq. (2) at normal incidence for  $m = -1$ . The result displayed in Fig. 4(b) (black dashed curve) fits well with the spectral position predicted by the numerical calculations. An additional peak resulting from the coupling of the guided mode to a higher order diffracted mode ( $m = -2$ ) appears for a grating period  $p$  over 425 nm as shown in Fig. 4(b) (black solid line).

The attribution of the resonance  $C_E$  to an eigenmode of the ZnO:Al/a-Si:H/Ag waveguide also explains the evolution of the total absorption spectrum when the a-Si:H layer thickness  $h_s$  varies. Indeed, the effective index of the guided mode increases with the thickness of the guiding layer, leading thereby to a shift of  $\lambda_{C_E}$  towards higher wavelengths. This is in good agreement with the spectral shift observed in Fig. 3(b).

Finally, it is worth noticing that the absorption peak at  $\lambda = 770$  nm for TM polarization, labelled  $C_M$ , can also be attributed to a guided mode supported by the a-Si:H layer. This resonance involves surface plasmons propagating at the a-Si:H/Ag interface thereby leading to parasitic absorption in the metallic mirror. As shown in Fig. 1, it leads to an absorption peak at an energy below the electronic bandgap of the absorber material. In the following, we show that this resonance can be shifted by the addition of a ZnO:Al buffer layer between the absorber layer and the back mirror and hence contribute to the generation of photocurrent in the structure (see subsection 4.2).



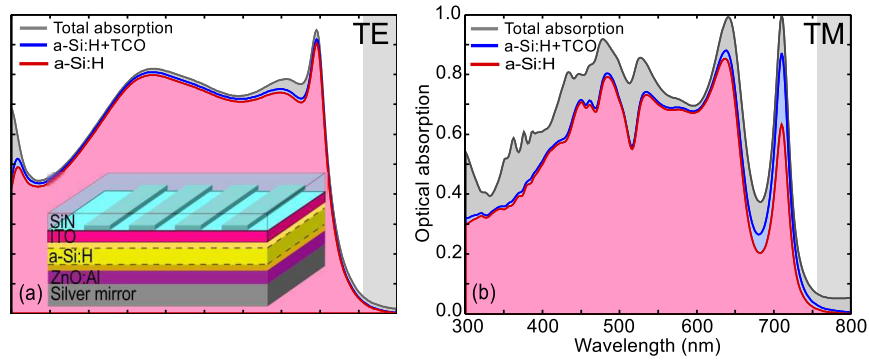


Fig. 5. Numerically computed optical absorption in each material of an ultra-thin a-Si:H solar cell for an excitation under TE (a, left) and TM (b, right) polarizations at normal incidence (red curve: absorption only in a-Si:H; blue curve: absorption in a-Si:H and the ITO and ZnO:Al spacing layers; grey curve: total absorption). The bandgap of amorphous silicon is shown in grey. Inset of Fig. (a): Sketch of the structure investigated: solar cell made of a  $\text{Si}_3\text{N}_4(\text{Ag})/\text{ITO}/\text{a-Si:H}/\text{ZnO:Al}/\text{Ag}$  stack with a 90 nm-thick p-i-n a-Si:H absorber layer. A 1D silver grating (thickness=20 nm, width=80 nm and period=200 nm) is embedded in the front  $\text{Si}_3\text{N}_4$  layer. Other geometrical parameters are  $h_{\text{Si}_3\text{N}_4}=60$  nm,  $h_{\text{ITO}}=10$  nm,  $h_{\text{ZnO:Al}}=15$  nm.

## 4. Application to ultra-thin amorphous silicon solar cells

### 4.1. Description of the complete cell

A complete photovoltaic cell is described in the inset of Fig. 5(a). The a-Si:H active layer is composed of a p-i-n junction, the influence of the doping on the refractive index of the material is neglected in this analysis. Two additional spacing layers are inserted above (ITO) and below (ZnO:Al) the a-Si:H layer to prevent metal diffusion in the absorbing layer. As shown in section 3 for the simplified structure, the use of the 1D silver grating leads to a multi-resonant and broadband absorption spectrum. The top ZnO:Al layer is replaced by a non-absorbing material (silicon nitride,  $\text{Si}_3\text{N}_4$ ). The top contact is then formed by the ITO spacing layer and the metallic grating, resulting in a reduction of optical absorption in the top layers of the structure at short wavelengths.

### 4.2. Design rules and influence of the ZnO:Al buffer layer

In section 3, we have identified the role of each geometrical parameter of the structure in the absorption resonances. This analysis provides guidelines for the design of the complete solar cell depicted in the inset of Fig. 5(a), as summarized in Table 1. The top anti-reflection layer ( $\text{Si}_3\text{N}_4$ ) thickness is set at 60 nm for a resonance at 450-500 nm. The thickness of a-Si:H layer is 90 nm and contributes to absorption enhancement in the 600-650 nm wavelength range. With a period of 200 nm, the grating leads to the excitation of guided modes in both TE and TM polarizations at a wavelength close to 700 nm.

We now investigate the influence of the two additional spacing layers. The influence of the ZnO:Al layer thickness on the absorption in the a-Si:H layer is displayed in Fig. 6(a) for TM polarization. In Ref. [27], Haug et al. reported that the ZnO:Al buffer layer between the a-Si:H absorber layer and the back silver mirror could have a beneficial effect on the absorption in the active layer. Let us compare the resonance labelled  $C_M$  in Fig. 1 to the absorption peak, at  $\lambda_G = 709$  nm in Fig. 6(a). Figures 6(b) and 6(c) display the electric field intensity maps corresponding to these two peaks. In both cases, the maximum field intensity is located within the

Table 1. Influence of the geometrical parameters of the structure shown in the inset of Fig. 5(a).

Geometrical parameter	Resonance type	Spectral range
Anti-reflection layer thickness	Vertical Fabry-Perot resonance in the top layer	450-500 nm
a-Si:H layer thickness	Vertical Fabry-Perot resonance in a-Si:H layer	600-650 nm
Grating period	Excitation of guided modes	650-750 nm

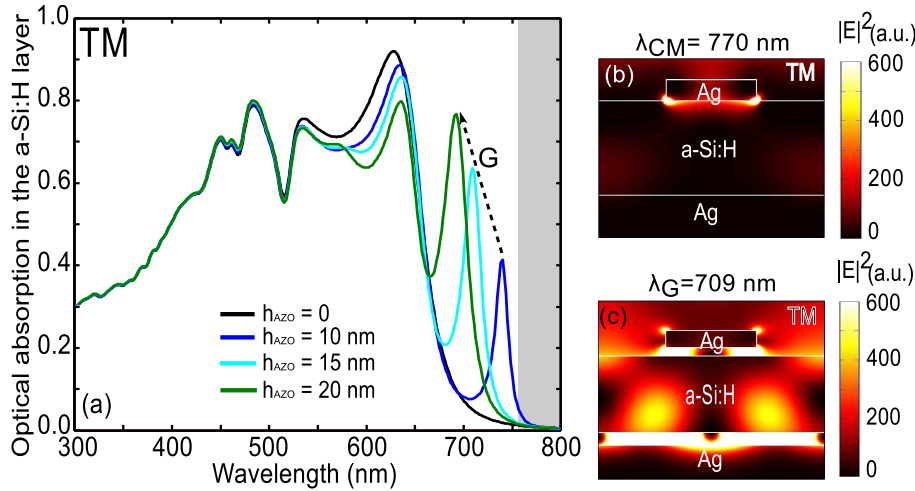


Fig. 6. (a) Evolution of the absorption in the a-Si:H layer for the complete cell as a function of the ZnO:Al layer thickness  $h_{AZO}$  for a TM polarized light at normal incidence. (b, c) Electric field intensity maps for an excitation at  $\lambda_{CM} = 770$  nm (simplified structure)(b) and  $\lambda_G = 709$  nm (complete cell)(c) at normal incidence for a TM polarization.

absorber layer. This agrees with the attribution of these peaks to a low energy guided mode observed under TM polarization. Besides, adding a low index buffer layer leads to a decrease of the effective index of the guided mode. This is consistent with the shift towards shorter wavelengths observed in Fig. 6(a) when  $h_{ZnO:Al}$  increases. The thickness of the buffer layer allows us to tune the spectral position of the peak corresponding to the guided mode G. However, increasing  $h_{ZnO:Al}$  induces a decrease of the absorption intensity at  $\lambda = 635$  nm because of increased absorption losses in the buffer layer, as evidenced in Fig. 6.

Therefore, the buffer ZnO:Al layer thickness is fixed to the value of 15 nm in order to achieve an optimal broadband absorption spectrum favored by a lower spectral position of the peak while limiting the fraction of incident photons absorbed in the buffer layer. Finally, the thickness of the ITO spacing layer between the metallic grating and the a-Si:H layer is chosen to be as low as possible ( $h_{ITO} = 10$  nm) to avoid parasitic losses in this layer.

The optical response of the resulting structure is shown in Figs. 5(a) and 5(b). The multi-resonant absorption spectra are very similar to those obtained for the simplified reference structure described in section 2. The absorption peaks at short wavelengths ( $\lambda \leq 700$  nm) are due to Fabry-Perot resonances in the  $Si_3N_4$  layer and a-Si:H layers. At long wavelengths, close to the a-Si:H bandgap, sharper peaks corresponding to resonances  $C_E$  (TE) and  $C_M$  (TM) of the simplified structure (see subsection 3.3) are evidenced.

### 4.3. Predicted performances of the cell

In section 3, the analysis of the multi-resonant mechanism was performed by considering the total absorption in the whole structure. In Figs. 5(a) and 5(b), we show the absorption fractions in each material constituting the solar cell for TE and TM polarizations. For the absorption peaks at  $\lambda = 636$  nm and 709 nm in TM polarization, perfect absorption is achieved in the structure: the critical coupling condition is achieved for these two resonances [28]. However, as shown in Fig. 5(b), there are non negligible parasitic absorption losses in the metallic grating in TM polarization.

We used the absorption spectrum in the a-Si:H active layer (red curve) to calculate the theoretical short-circuit current density of the cell, assuming that all photogenerated carriers are collected [19]. A  $J_{SC}$  of 14.6 mA/cm<sup>2</sup> is predicted for a cell with a 90 nm-thick a-Si:H absorber layer. In order to evaluate the global performances of the cell, we used state-of-the-art values [7] for the open-circuit voltage ( $V_{OC} = 0.88$  V) and fill factor (FF = 0.7) leading to a theoretical conversion efficiency of 9%.

## 5. Conclusion

In summary, we have studied the multi-resonant absorption mechanism achieved in ultra-thin a-Si:H solar cells with a patterned metallic front contact. The three resonances observed for TE and TM polarizations are analyzed by simple models, and attributed to Fabry-Perot resonances in the ZnO:Al and a-Si:H layers, and the excitation of guided modes via grating coupling. This detailed analysis is a powerful tool to optimize a design without exploring the whole parameter space. We have generalized this approach to a complete a-Si:H solar cell. An additional ZnO:Al buffer layer is used to tune the absorption spectrum and reduce the parasitic losses in the metallic parts. This multi-resonant approach is broadly applicable to other thin-film solar cell materials such as GaAs or CIGS. This work could guide the optical design of solar cells with multi-resonant light trapping schemes.

## Acknowledgments

The authors would like to thank A. Cattoni and J. F. Guillemoles for fruitful discussions. This work was partially supported by the ANR projects ULTRACIS and NATHISOL.